A 30-year ocean front dataset from 1993 to 2023 for the Northwest Pacific Ocean based on deep learning

Yuan Niu[1], Xuefeng Zhang[1], Dianjun Zhang[1]

[1]School of Marine Science and Technology, Tianjin University, Tianjin 300072, China

Correspondence to: Dianjun Zhang (zhangdianjun@tju.edu.cn)

Abstract. Ocean fronts are critical interfaces between different water masses and profoundly influence atmosphere–ocean interactions, weather systems, marine ecosystems, and climate regulation. Accurate and long-term observations of ocean fronts are essential for advancing studies in meteorology, oceanography, and climate science. However, no publicly available, long-term ocean front dataset currently exists, and the existing detection methods often rely on time-consuming manual labeling or traditional algorithms with limited accuracy in complex frontal regions. In this study, we release the first publicly available 30-year ocean front dataset (1993–2023) for the Northwest Pacific, which was generated by applying a deep learning framework (Mask R-CNN) to daily sea surface temperature (SST) fields with manually annotated samples for model training. The model was trained utilizing both L3 remote sensing satellite SST data and the GLORYS12V1 L4 reanalysis SST product. The dataset provides pixel-level frontal boundaries along with the associated attributes, including the position, intensity, and width, stored in NetCDF-4 format at a 1/12° spatial and daily temporal resolution. An accuracy evaluation shows that the mean average precision (mAP) exceeds 0.90, and compared with traditional gradient methods, the errors in front width and intensity are smaller. The dataset offers three main contributions: (1) It fills a critical gap by providing a standardized, long-term ocean front product; (2) it serves as a ready-to-use training resource for deep learning models that greatly reduces the need for manual labeling; and (3) it provides benchmark samples for validation and intercomparison of other ocean front detection products. This dataset supports robust investigations of the seasonal-to-interannual frontal variability and provides a valuable foundation for applications in meteorology, ecosystems management and climate change research.

1 Introduction

Ocean fronts refer to narrow transition zones between two or more water masses with significantly different properties, where oceanographic parameters such as the temperature, salinity, and water colour experience sharp changes. It can be characterized by the horizontal gradient of the sea surface temperature (Chen, 2009; Wang and Wang, 2015). As an important intersection between the atmosphere and the ocean, ocean fronts hold a significant position in the field of Earth science (Gruber et al., 2011; Azevedo et al., 2021). From extreme weather events to changes in marine ecosystems to the stability of the global climate system, ocean fronts are important in multiple fields (Belkin et al., 2009), and ocean fronts detection is crucial for meteorological and climate research (Chronis, 2021). By accurately identifying and tracking ocean fronts, it is possible to better understand the dynamics of climate and weather systems, thereby providing early warning for extreme weather events (Saldías et al., 2021). The identification of(Azevedo et al., 2021) ocean fronts can help us better understand the Earth's climate and ecosystems, providing support for global climate change research (Ruiz et al., 2019).

The data sources for ocean front extraction include SeaWiFS water colour data (Belkin and O'reilly, 2009), MODIS sea surface temperature (SST) , and AVHRR SST remote sensing image data (Shaw and Vennell, 2001). The main methods for front detection are population-based (Cayula and Cornillon, 1992; Nieto et al., 2012; Roa-Pascuali et al., 2015; Diehl et al., 2002) and gradient-based (Oram et al., 2008; Davis, 1975). Cayula and Cornillon proposed the single-image edge detection (SIED) algorithm based on histogram analysis. This algorithm demonstrates effective detection performance and has been widely applied in ocean front detection. The gradient algorithm is a commonly used ocean front detection method and uses the Sobel operator, Prewitt operator, Laplacian operator, and other gradient operators. Ping et al. (2014) proposed an ocean front detection method based on threshold intervals and Bayesian decision theory. This method uses the Sobel operator to compute the gradient map of SST images and determines the threshold interval by using a gradient histogram, ultimately achieving ocean front detection (Ping et al., 2014). Traditional gradient threshold methods rely on setting a threshold value to identify ocean fronts manually (Wang and Liu, 2009). However, the selection of this threshold is subjective and lacks a standardized criterion. In addition, different researchers or studies may choose different threshold values, leading to inconsistency and variability in the detected ocean fronts.

With the continuous deepening of deep learning research, convolutional neural networks (CNNs) and R-CNNs have achieved great success in various scenarios, such as image detection, speech detection, and target detection (Yang et al., 2018; Chen et al., 2020; Reichstein et al., 2019). On this basis, the Mask R-CNN network achieved pixel-level instance segmentation of images (He et al., 2017). Lima et al. (2017) proposed a fine-tuning neural network for ocean front detection based on previous research to address practical situations in which deep networks such as AlexNet, Caffe Net, GoogLeNet, and VGGNet are prone to overfitting under limited training data. Sun et al. (2019) proposed a multiscale detection framework for ocean front detection and fine-grained positions, and Li et al. (2019) proposed an ocean front detection network based on the CNN to address the weak edges of ocean fronts. To detect more precise ocean fronts, the network fuses the convolutional features at each stage and uses the Intersection over Union (IoU) loss function and binary cross-entropy loss function to fix model errors. Xie et al. (2021) used LSENet to detect and locate multiple ocean fronts in colour SST gradient maps, achieving an ocean front detection breakthrough with a mean Dice Similarity Coefficient (mDSC) (Dice, 1945) greater than 90%, and Li et al. proposed a deep learning model with a U-Net architecture that is designed to detect and locate significant frontal zones in grayscale sea surface temperature images and successively developed a bidirectional edge detection network (BEDNet)(Li et al., 2020) and weak edge identification network (WEIN) (Li et al., 2022). Niu et al. designed a multi-scale simple and quick net (SQNet) model to identify the positions of ocean fronts based on their characteristics (Niu et al., 2023) , and Felt et al. proposed machine learning (ML) models to detect temperature and chlorophyll ocean fronts from unprocessed and radiometrically uncorrected satellite imagery via transfer learning from existing models for edge detection (Felt et al., 2023).

Table 1. Overview of the existing classic research on ocean front extraction based on deep learning approaches

Author	Experimental area	Network model	Result accuracy	Advantages	Limitations
Lima et al. (2017)	Small regions	CNN	88%	Method involves CNNs and transfer learning via finetuning	Low image resolution
Sun et al. (2019)	Small regions	AlexNet	90%	Six scanning scales	The experimental area is too small
Li et al. (2022)	30-34°N, 132-140°E	U-Net	90%	Small time cost	The detection effect of complex sea areas needs to be verified
Niu et al. (2023)	The coast of China and the Gulf of Mexico	SQNet	90%	Based on a multi-scale	The research area is small
Felt et al (2023)	Coastal regions	CNN	90%	Improved computational efficiency	Too few samples in the dataset

With the application of deep learning in the field of image detection (Nogueira et al., 2016), and in view of the shortcomings of traditional gradient threshold methods, ocean front detection algorithms based on deep learning have become a research hotspot. Sufficient training samples are the basis of target detection based on deep learning. The integration of ocean front detection and deep learning requires significant computational and integration costs, while training data remain scarce, making dataset construction particularly difficult. Therefore, considering the small amount of data and the lack of standardized criteria in traditional methods, this paper proposes a new automatic ocean front detection method that applies Mask R-CNN to ocean front detection and then achieves high-precision detection of ocean fronts via multiple iterative training steps and parameter correction.

2 Study area and data

The study area for this research spans a latitudinal range of 0° to 50°N and a longitudinal range of 100° to 150°E (Fig. 1). The worldwide ocean eddy-resolving (1/12° horizontal resolution, 50 vertical levels) reanalysis encompassing altimetry data (1993 forward) was provided by the Copernicus Marine Environment Monitoring Service (CMEMS) and is available as the GLORYS12V1 product. It is based largely on the current real-time global forecasting CMEMS system. The model components include the Nucleus for European Modelling of the Ocean (NEMO) platform driven at the surface by the European Centre for Medium-Range Weather Forecasts (ECMWF) ERA-Interim and the ERA5 reanalyses for recent years. Observations are assimilated by means of a reduced-order Kalman filter. The sea surface temperature, sea ice concentration, in situ temperature and salinity vertical profiles are jointly assimilated along-track altimeter data. Moreover, a 3D-VAR scheme provides a correction for the slowly evolving large-scale biases in temperature and salinity. This product includes daily and monthly mean files for the temperature, salinity, currents, sea level, mixed layer depth and ice parameters. The global ocean output files are provided on a standard regular grid at 1/12° (approximately 9 km) and 50 standard levels. The data used in this work were sourced from the daily average sea surface temperature dataset, covering a period of 30 years from January 1, 1993, to December 31, 2023. The units are °C; the temporal resolution is daily; and the spatial resolution is 1/12°. The specific parameter information for the data is shown in Table 2, and the dataset is accessible via DOI: 10.48670/moi-00021.

To augment the training dataset, we also utilized the ODYSSEA Global Ocean - Sea Surface Temperature Multi-sensor L3 Observations product from CMEMS. This product provides the daily foundation sea surface temperature (Foundation SST) derived from multiple satellite sources. The dataset consists of a fusion of sea surface temperature observations from multiple satellite sensors, mapped on a global 0.1° × 0.1° resolution grid on a daily basis. It includes observations from polar-orbiting satellites (NOAA-18 & NOAA-19/AVHRR, METOP-A/AVHRR, ENVISAT/AATSR, AQUA/AMSR-E, TRMM/TMI) and geostationary satellites (MSG/SEVIRI, GOES-11). Prior to merging, the observations from each sensor were intercalibrated using a bias correction based on a multi-sensor median reference to correct large-scale cross-sensor biases. The downloaded data covers the period from January 1, 2021, to December 31, 2022. The dataset is available via DOI: 10.48670/moi-00164.

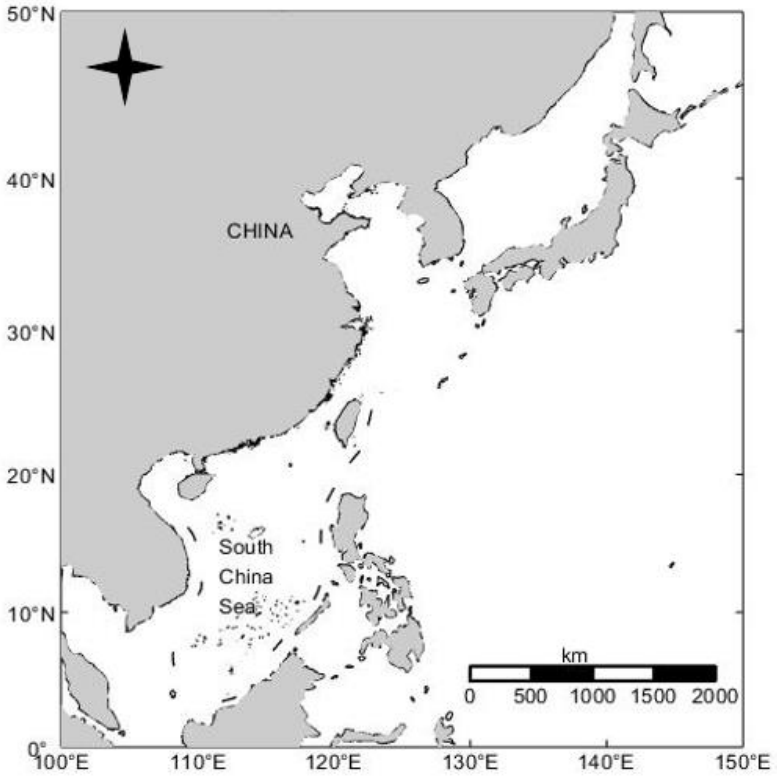

Figure 1. Location of the study area

Table 2. Data parameter description

Information	Details
Full Name	Global Ocean Physics Reanalysis
Product ID	GLOBAL_MULTIYEAR_PHY_001_030
Source	Numerical models
Spatial extent	Global Ocean
Spatial resolution	0.083° × 0.083°
Temporal extent	1 Jan 1993 to 31 Dec 2023
Temporal resolution	Daily, Monthly
Elevation levels	50
Processing level	Level 4
Variables	Sea water potential temperature (T)
Feature type	Grid
Blue markets	Polar environment monitoring Policy & governance Science & innovation

	Extremes, hazards & safety
	Coastal services
	Natural resources & energy
	Trade & marine navigation
Projection	WGS 84 (EPSG:4326)
Data assimilation	In-Situ TS Profiles
	SST
Update frequency	Annually
Format	NetCDF-4
Originating centre	Mercator Ocean International

3 Methods

3.1 Gradient calculation

We estimate the SST gradient magnitude *G* from the gridded SST field *T(i,j)* using centered finite differences:

$$D_x(i,j) = \frac{T(i,j+1) - T(i,j-1)}{2\Delta x} \quad (1)$$

$$D_y(i,j) = \frac{T(i+1,j) - T(i-1,j)}{2\Delta y} \quad (2)$$

$$G(i,j) = \sqrt{D_x(i,j)^2 + D_y(i,j)^2} \quad (3)$$

Here Δx and Δy are the grid spacings (in km), and (*i*,*j*) denotes the grid indices.

3.2 Data labels

Ocean fronts were manually delineated using Labelme (Wada, 2021), a Python-based open-source image annotation tool (https://doi.org/10.5281/zenodo.5711226). For each SST gradient map, polygon boundaries were drawn around visually continuous front features. Multiple polygons may be drawn within a single map, as multiple ocean fronts can appear in one image. Each annotated map was saved as a Labelme JSON file containing the polygon coordinates and corresponding metadata.

The annotated SST gradient maps were derived from the 30-year dataset created using the gradient method (Section 3.1), based on the GLORYS12V1 L4 reanalysis and L3 satellite SST data described in Section 2. The labeled dataset comprises 5,000 samples, where each sample consists of one SST gradient map and its associated JSON annotation file.

3.3 Construction of the Mask R-CNN model

Mask R-CNN extends Faster R-CNN by adding a branch parallel to the existing target detection frame to predict the target mask. Mask R-CNN has three outputs: a class label, a bounding-box offset and the target mask. The difference between the target mask and the class-box output is that more refined extraction of the target's spatial layout is needed. The network architecture diagram of Mask R-CNN is shown in Fig. 2. Mask R-CNN is an instance segmentation network that takes an input image of arbitrary size, predicts class labels, bounding boxes, and pixel-level masks for each detected object. The success of this architecture is based on several factors, such as the availability of large datasets, increased computing power, and the availability of GPUs. It also depends on the implementation of additional techniques, such as dropout, data augmentation to prevent overfitting, and rectified linear units to accelerate the training phase.

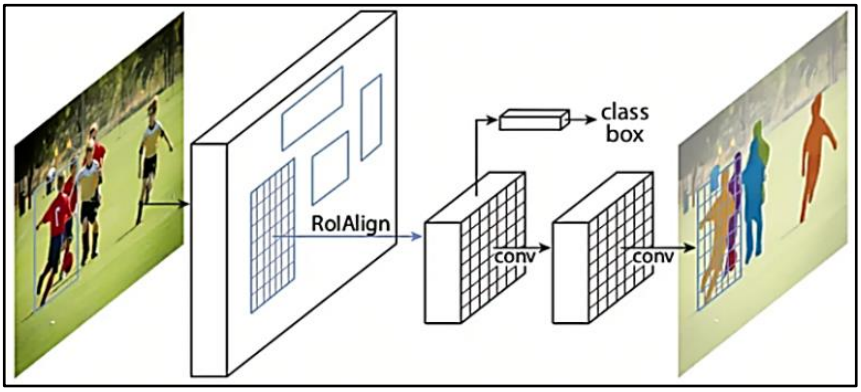

Figure 2. Mask R-CNN network architecture (He et al., 2017)

The residual neural network (Res-Net) and feature pyramid network (FPN) are the key networks used to extract features in Mask R-CNN. Res-Net is a residual learning framework used to reduce the burden of network training, and the FPN extracts region of interest (ROI) features from different feature levels according to the size of the features. A region generation network (RPN) is used to generate candidate regions. Then, ROI Align collects the image features and candidate region features as the input to the subsequent full connection layer and then determines the target category.

Applying deep learning methods to ocean front detection is challenging because fronts have significant visual similarity and are indistinguishable in colour and shape. Ocean fronts are regions in which sharp transitions in oceanic properties such as temperature, salinity and density occur. These fronts are critical for understanding the dynamics of the ocean and global climate system. However, detecting and characterizing these fronts is challenging due to their complex and dynamic nature. In particular, the visual similarities among different fronts can make them difficult to distinguish based on gradient magnitude patterns and shape alone. Deep learning methods offer a promising approach to overcome these challenges. By leveraging large datasets of oceanographic data, including satellite imagery and in situ measurements, deep learning models can learn to identify the patterns and features that are characteristic of different types of ocean fronts. These models can then be used to classify and characterize fronts with high accuracy and efficiency. To develop effective deep learning models for ocean front detection, it is essential to carefully curate and preprocess the training data to ensure that it is representative of the range of oceanographic conditions and front types that may be encountered in the real world. Additionally, the choice of neural network architecture and training parameters significantly affect the performance of the model, and careful tuning and evaluation are required to ensure optimal results.

In our framework, ocean fronts are represented as a pixel band with finite width (i.e., a narrow binary mask region), rather than a single-pixel wide line or a bounding box enclosing a high-gradient region. This approach better reflects the physical nature of the front as a transition zone between two water masses. As a connected region, it is directly compatible with the instance segmentation mask output by Mask R-CNN and the IoU area calculation. While the front is geographically quasi-

linear, modelling it as a "finite-width band" transforms the problem into a region segmentation task. The task of Mask R-CNN is to predict a corresponding binary mask for each front instance. Then, the IoU is calculated based on the area overlap between the predicted mask and the ground-truth mask, which is used to evaluate the detection performance. This process follows the standard evaluation procedure for instance segmentation. Additionally, we designed a non-maximum suppression (NMS) algorithm based on spatial location and mask similarity specifically for merging duplicate detections of the same front segment in overlapping areas with adjacent tiles and for connecting broken parts across boundaries, thereby forming a complete and continuous front vector.

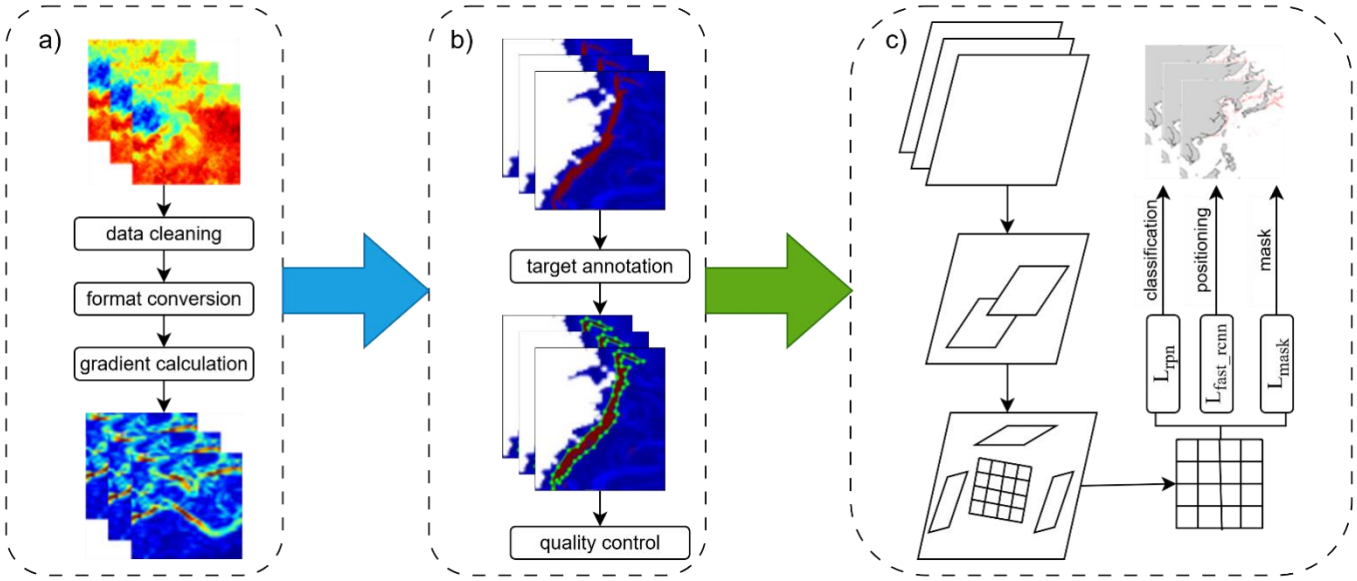

Figure 3. Network architecture diagram for identifying ocean fronts using Mask R-CNN

The Mask R-CNN loss involves the addition of the loss on the Mask branch on top of Faster R-CNN, which is described as follows:

$$\text{Loss}=L_{rpn}+L_{fast\_rcnn}+L_{mask} \tag{4}$$

L_{rpn} generates objects by proposing potential bounding box regions in the image. The L_{fast_rcnn} network extracts the proposed region from the RPN and performs region classification and bounding box regression, and the L_{mask} loss measures the accuracy of the predicted mask by comparing it with the actual mask. By combining these three losses, Mask R-CNN's overall loss function guides the network to simultaneously perform accurate region proposals, object classification, bounding box regression and instance segmentation. The network learns to balance these different objectives during training to improve its performance in tasks such as object detection and instance segmentation.

The loss function is usually associated with optimization problems, for which it is employed as a learning criterion; that is, the model is solved and evaluated by minimizing the loss function. According to the above task description, the loss function of RPN training consists of two parts: classification loss and position regression loss.

$$L(\{p_i\},\{t_i\}) = \frac{1}{N_{cls}} \sum_i L_{cls}(p_i, p_i^*) + \lambda \frac{1}{N_{\text{reg}}} \sum_i p_i^* L_{reg}(t_i, t_i^*) \tag{5}$$

$L(\{p_i\},\{t_i\})$ refers to the entire loss function, which represents the total loss of the model. $\frac{1}{N_{cls}}$ is a scalar that represents the normalization factor of the classification loss term, where N_{cls} denotes the number of categories in the classification task. $\sum_i L_{cls}(p_i, p_i^*)$ represents the sum of the classification loss terms, which is usually used to measure the performance of the

model in classification tasks. The classification loss involves each sample i, where p_i is the predicted probability distribution of the model and p_i^* is the probability distribution of the actual label. L_{cls} is usually a cross-entropy loss or other classification loss function. λ is a nonnegative constant used to balance the classification loss term and the regression loss term, and $\frac{1}{N_{\text{reg}}}$ is the normalization factor for the regression loss term, where N_{reg} represents the number of samples. $\sum_i p_i^* L_{reg}(t_i, t_i^*)$ represents the sum of the regression loss terms. The regression loss for each sample i is involved, where t_i is the predicted regression value of the model and t_i^* is the actual regression target value.

During the training process, the gradient image of the SST data on the target date was selected to detect and extract ocean fronts. An overview of the experimental workflow is provided in Fig. 4, which illustrates the sequential steps involved in detecting and evaluating ocean fronts by using the Mask R-CNN model. This flow chart helps to visualize the process and highlights the key stages in the experiment. The process can be summarized as follows:

1) Acquisition of SST Data: The experiment commenced with the acquisition of SST data for the study area, specifically incorporating both the L3 remote sensing satellite SST data and the GLORYS12V1 L4 reanalysis SST product.

2) Preprocessing: the L3 remote sensing satellite SST data were interpolated to a 1/12° grid to unify the spatial resolution with the reanalysis product. Furthermore, considering that satellite SST observations are frequently compromised by cloud cover, we screened the dataset to identify and select valid data within the study area, ensuring the integrity of the samples used for analysis.

3) Gradient calculation: The gradient of the SST image was calculated to identify areas of rapid temperature change, which are indicative of ocean fronts. The gradient represents the spatial variation in temperature across the image.

4) Gradient image: The calculated gradient values were used to generate a gradient image, where higher gradient values correspond to stronger temperature gradients and potential ocean fronts. This image provides a visual representation of the potential ocean fronts locations.

5) Model training: The Mask R-CNN model was trained by using the gradient image as input. The model learned to identify and classify ocean fronts based on the patterns and features present in the gradient image. This step involves training the model on a large dataset with labeled ocean fronts samples.

6) Detection results: The trained model was applied to the entire SST image dataset to detect and localize ocean fronts. The model analyzed each image and identified regions in which ocean fronts were present.

7) Evaluation of the results: The detection results were evaluated to assess the performance and accuracy of the Mask R-CNN model in terms of detecting ocean fronts. Various metrics, such as the precision, recall, and F1 score, were calculated to measure the model's effectiveness in terms of correctly identifying and locating ocean fronts.

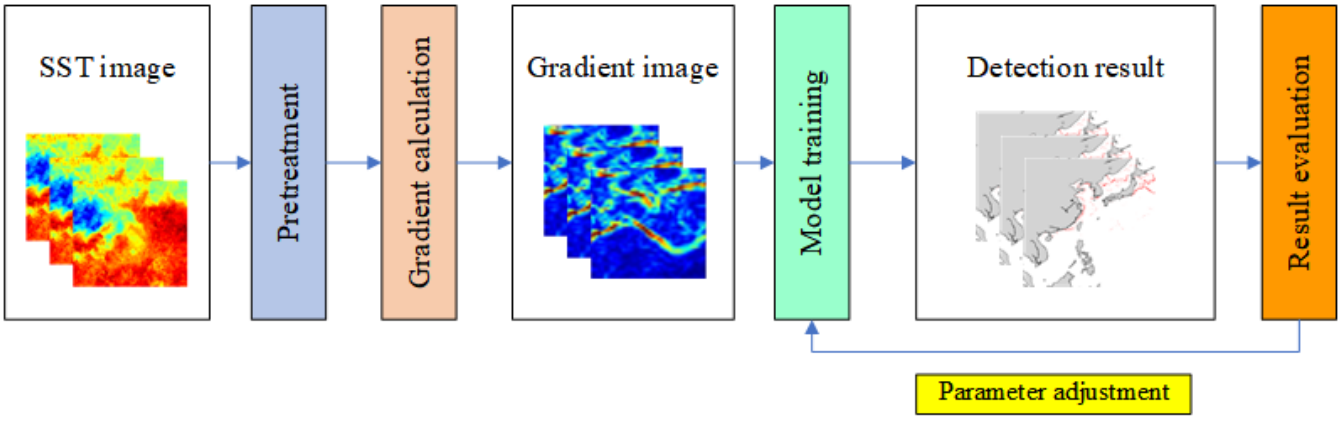

Figure 4. Flow chart of experiment

3.4 Mathematical testing methods

The mean average precision (mAP) was chosen as the evaluation metric. First, the accuracy of the front was represented by the IoU (Intersection over Union), and the general threshold was set to 0.5, which means that if the IoU ≥ 0.5, the detection is considered correct. Then, by using the recall as the horizontal axis and the accuracy as the vertical axis, the P-R curve was obtained. Ideally, both P and R can achieve results that are infinitely close to 1 at the same time. Therefore, ideally, the area covered under the P-R curve is infinitely close to 1. The area below P-R is called the average accuracy of ocean front detection, known as the AP (Average Precision). The average of multiple APs is the mAP. The definitions of the IoU, P, R, and AP are as follows:

$$loU = \frac{\text{Area of Overlap}}{\text{Area of Union}} \tag{6}$$

$$\mathrm{P} = \frac{TP}{TP+FP} \tag{7}$$

$$\mathrm{R} = \frac{TP}{TP+FN} \tag{8}$$

$$AP = \int_0^1 \mathrm{P}\,(\,\mathrm{R}\,)\,\mathrm{dR} \tag{9}$$

In the equation, the area of overlap refers to the intersection of two prediction boxes, and the area of union is the union of two prediction boxes. TP denotes predicted ocean-front instances that correctly match a ground-truth front, FP denotes predicted instances that do not correspond to any ground-truth frons, and FN denotes ground-truth fronts that were not detected by the model.

4 Results and discussion

4.1 Gradient calculation results

To generate the frontal indicator field, we first calculated the temperature gradient by using Eqs. (1) – (3). Fig. 5 shows the resulting field for January 2023, which highlights regions in which the sea surface temperature changes rapidly, revealing the spatial structure of ocean fronts. Warmer colours correspond to stronger transitions. This representation clearly outlines areas of active frontal variability and facilitates a straightforward visual assessment of their distribution and evolution during the month.

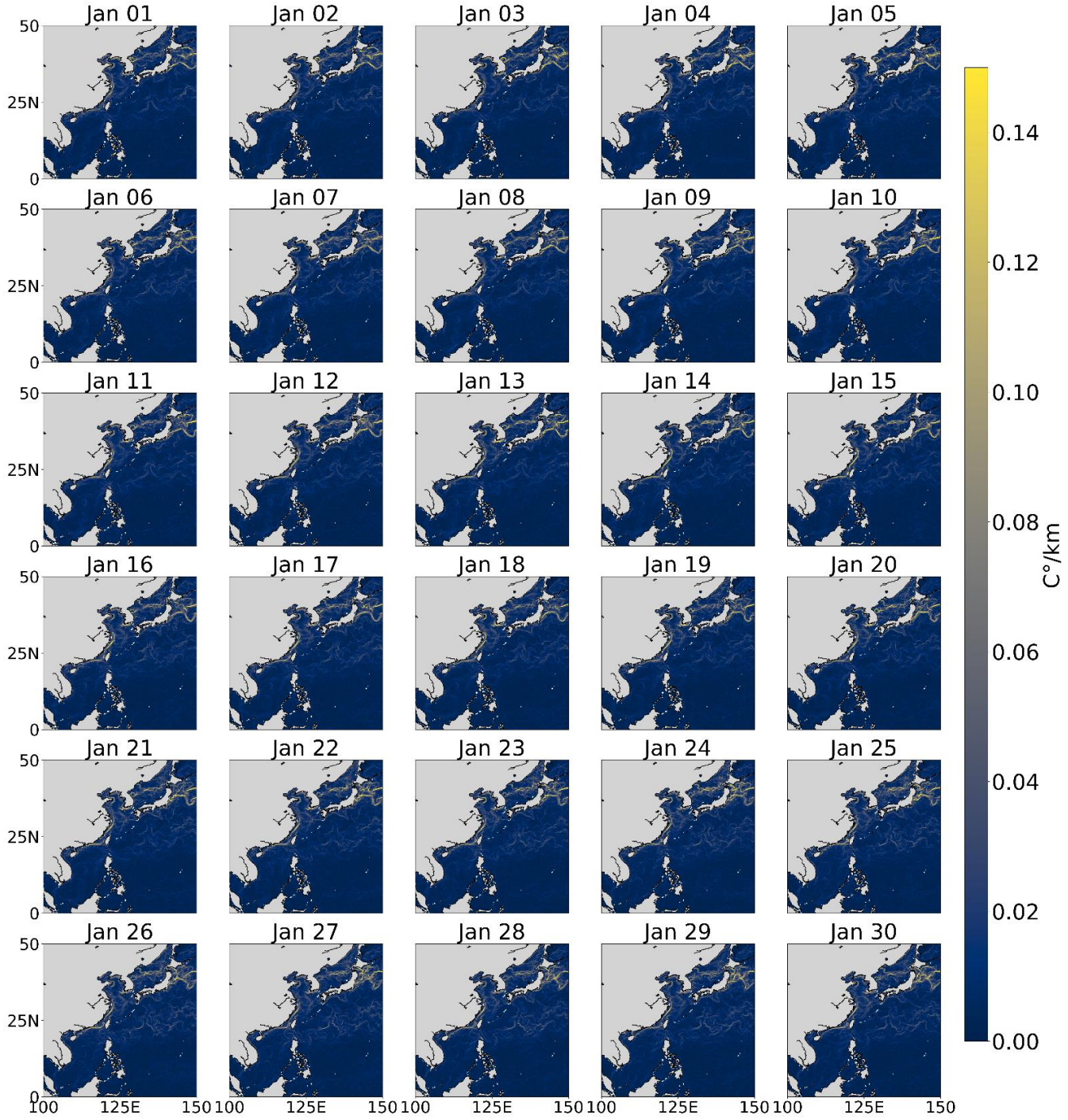

Figure 5. Gradient image of ocean fronts time series in January 2023

4.2 Image marking results

Sufficient training samples are essential for deep learning-based ocean front detection. However, ocean fronts appear as small-scale and weak-edge features in SST imagery, making it difficult to construct a large and effective training dataset, particularly in regions in which the frontal edges are diffuse or ambiguous. To address this limitation, we collected SST images from regions known to exhibit frequent global frontal activity and applied data augmentation and feature enhancement techniques. In addition, a frontal indicator field was derived from the SST data to highlight the frontal structures.

To create the labeled dataset (Fig. 6), each ocean front was manually annotated by using the Labelme software. Annotators outlined the frontal boundaries in the SST and gradient-enhanced images to generate polygonal masks representing individual fronts. These masks were then converted into COCO-style instance labels (i.e., JSON-formatted annotations containing polygon coordinates and instance-level segmentation information) to train the Mask R-CNN model (Lin et al., 2014).

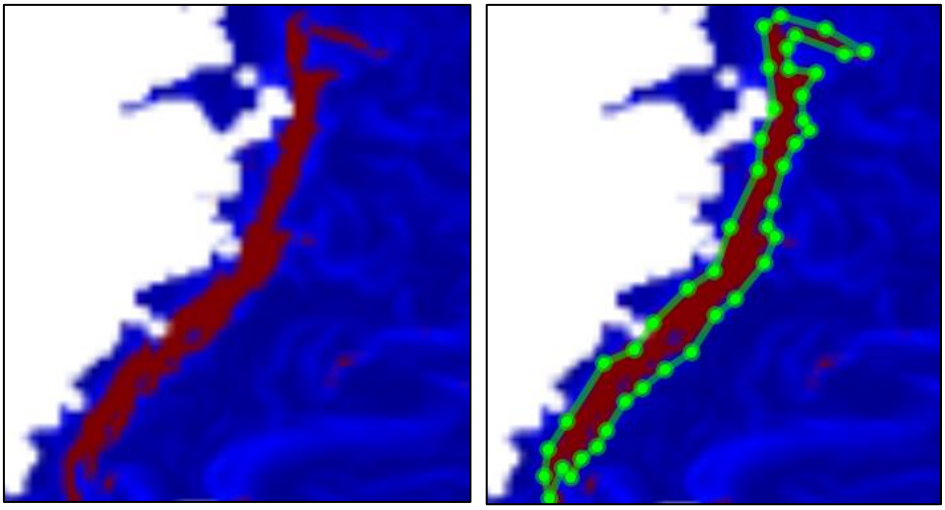

Figure 6. Comparison of the original temperature gradient image and its manual annotation for ocean fronts. Original temperature gradient image (left panel); manually annotated frontal masks (right panel).

4.3 Detection results of the model

In the field of deep learning, datasets are divided into three parts: a training set, a validation set, and a testing set. The data in the training set are used to construct the model, and the validation set is used to evaluate the predictive performance of each model and choose the model with the best performance. After selecting the model with the best accuracy via the validation set, the performance of the optimal model is evaluated on the test set. Notably, to ensure the accuracy of the evaluation, the test set data do not participate in the training process. The quality of the training dataset is the key to affecting the accuracy of the target detection model. To achieve the automatic extraction and learning of the high-level essential features of ocean fronts in temperature images, a multilevel network model was constructed, thereby achieving the automatic detection of ocean fronts. The entire process does not require manual intervention; thus, during the dataset construction process, multisource temperature data were used to ensure the diversity of training data and enhance the generalization ability of the model.

Mask R-CNN exhibits excellent feature learning, but it requires multiple adjustments of various network parameters to optimize the network and detection results and thus obtain the best ocean front detection model. The network parameters commonly adjusted in deep learning include the momentum, learning rate, batch size, weight attenuation ratio, number of iterations. The learning rate is usually set to 0.0002, the weight attenuation is typically set to 0.0005, and the batch size is set

to 2 due to memory limitations. The network parameter settings with the best detection accuracy are obtained primarily by adjusting the proportion of training and validation set, the learning rate, and the number of iterations.

To evaluate the data efficiency of the proposed model, we conducted comparative experiments by gradually decreasing the proportion of training set while increasing the proportion of validation set. For each data split, the model was trained with fixed hyperparameters (learning rate = 0.0002, batch size = 2, number of iterations = 1000), and the performance was evaluated on the corresponding validation set. As shown in Table 3, when the training set proportion decreased from 0.8 to 0.75, the average precision (AP) and average recall (AR) improved, suggesting that a moderate increase in validation set may help better assess model generalization. However, as the training proportion further decreased to 0.6, both AP and AR gradually declined, indicating that insufficient training data hinder the model's ability to learn representative features. Based on these observations, we selected a training/validation split of 75%/25% as a balance between training sufficiency and validation reliability. Hyperparameters were tuned using this validation set, and the final model performance was evaluated on a separate test set consisting of SST data from 2023, which was not used during model development. The test set results are reported in the subsequent section.

Table 3. Comparison of training model results under different training and validation splits

serial number	The proportion of training set	The proportion of validation set	Learning rate	Batch Size	Number of iterations	AP	AR
1	0.8	0.2	0.0002	2	1000	0.918	0.893
2	0.75	0.25	0.0002	2	1000	0.929	0.907
3	0.7	0.3	0.0002	2	1000	0.921	0.898
4	0.65	0.35	0.0002	2	1000	0.902	0.846
5	0.6	0.4	0.0002	2	1000	0.897	0.812

To verify the accuracy of the model's detection results, the model was tested by using the test dataset, and the mAP was calculated. The results were compared with the manually annotated results, and the IoU value was also computed. Additionally, to further improve the ocean front detection performance, the model parameters were continuously adjusted to enhance both the mAP and IoU. Finally, after 30,000 iterations, the trained network successfully demonstrated the ability to detect ocean fronts. The training loss and detection mAP according to different numbers of iterations are shown in Table 4.

As the number of training iterations increases from 5,000 to 30,000, the training loss decreases from 0.327 to 0.118, the IoU increases from 0.671 to 0.916, and the mAP improves from 0.680 to 0.920. These findings indicate that the network gradually learns better feature representation and classification capabilities during the training process, thereby improving its performance in detection tasks. Notably, although both the loss and detection accuracy significantly improved during training, the rate of loss reduction slows down after 30,000 iterations, whereas the detection accuracy continues to improve. This finding may indicate that the network has approached or reached its optimal performance on this dataset, and further training may result in only minor improvements. In summary, the loss and detection accuracy of the training network improve with an increasing number of training iterations, demonstrating that the network's performance in learning tasks gradually improves.

Table 4. Training network loss and detection accuracy rate

Iterations	loss	IoU	mAP
5000	0.327	0.671	0.680
10000	0.195	0.758	0.770
15000	0.156	0.820	0.830

20000	0.133	0.864	0.860
25000	0.127	0.871	0.880
30000	0.118	0.916	0.920
35000	0.120	0.897	0.903

Fig. 7 shows the detection results for ocean fronts based on the Mask R-CNN model in January 2023. Through the application of deep learning algorithms, the positions and shapes of ocean fronts were identified and displayed by using markers and contours. From the graph, it can be observed that the ocean front detection results based on deep learning algorithms can display obvious features. Furthermore, the position and shape of ocean fronts are clearly visible in the figure, indicating that the algorithm can effectively capture the spatial distribution of ocean fronts and accurately distinguish it from the surrounding sea area. Second, the ocean front detection results shown in the figure demonstrate the manifestation of small-scale information. Ocean fronts typically have complex shapes and variations, including slender strip structures and local eddies. Deep learning algorithms can capture these small-scale features, making the detection results more refined and continuous.

In addition, the ocean front detection results based on the Mask R-CNN model show good continuity over a time range. Ocean fronts shown in the figure exhibits a relatively stable distribution and evolution trend over time, indicating that the detection algorithm has high stability and reliability and can effectively track and analyse changes in ocean fronts.

To further test the accuracy of deep learning methods in terms of identifying ocean fronts, sea surface temperature data for April 2023 were used. The traditional gradient method was employed to obtain reference ocean front maps, against which the deep learning results were compared (Fig. 8). As shown, ocean fronts extracted by the deep learning model are highly consistent with those derived from the traditional gradient method, demonstrating the model's effectiveness in capturing frontal structures.

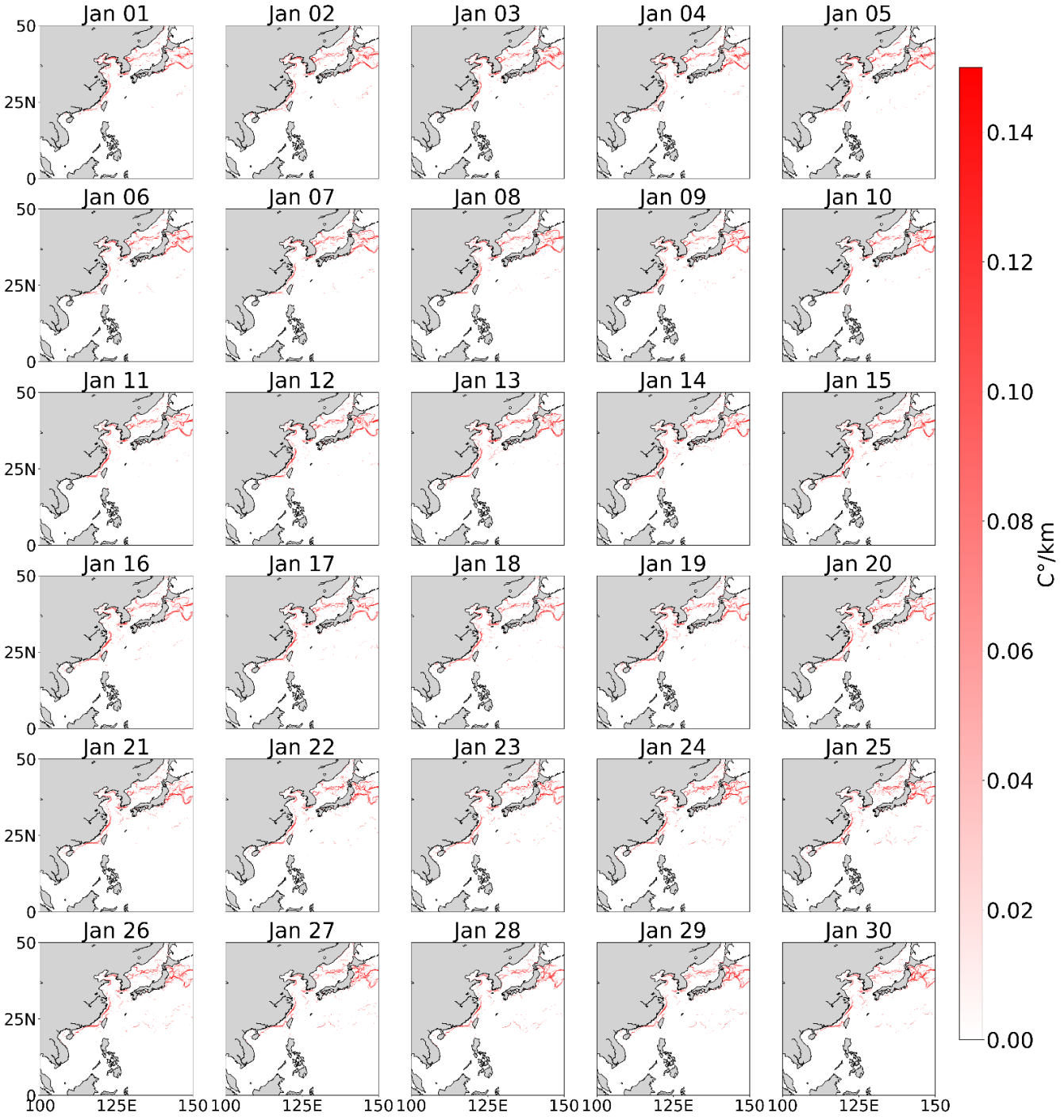

Figure 7. Identification Results of Ocean Front Time Series in January 2023

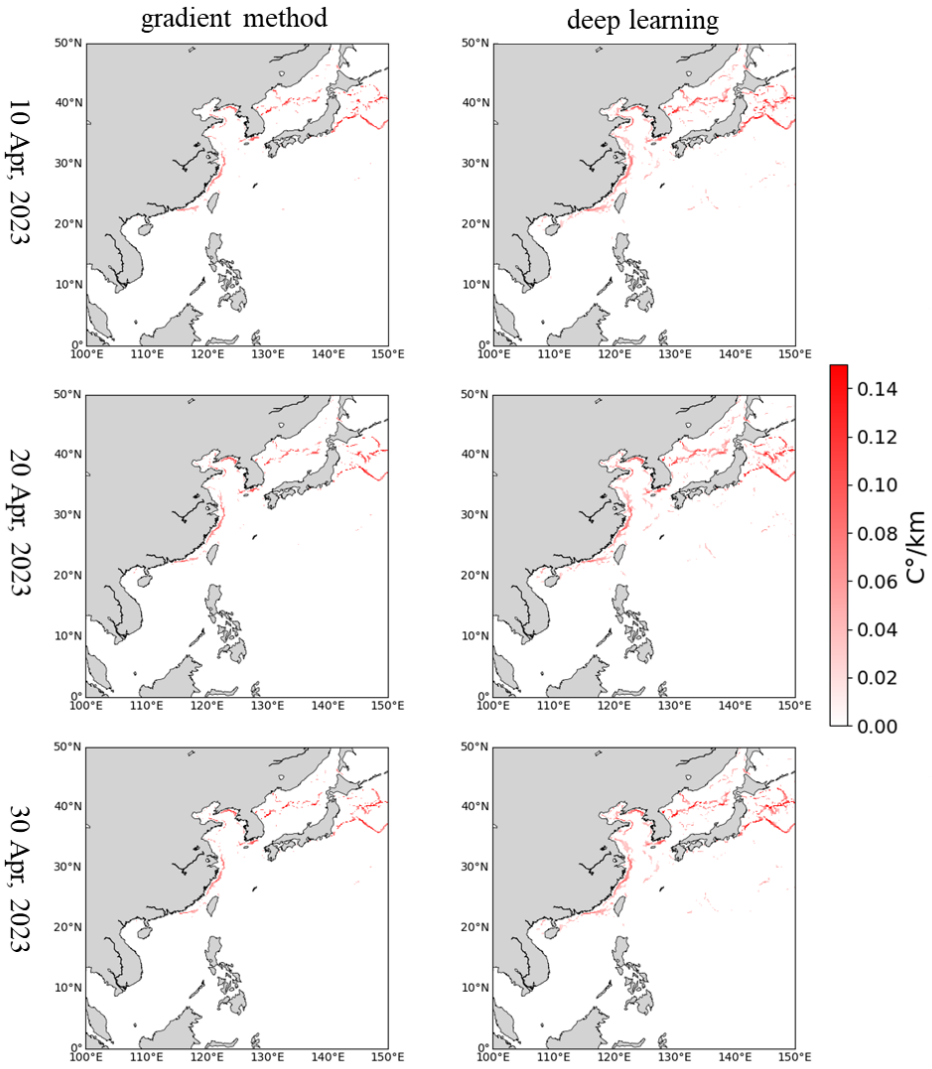

Figure 8. Comparison of Ocean Front Results in April 2023. (Left: Gradient method detection results; Right: Deep learning detection results)

Furthermore, based on the ocean front detection results, the intensity and width at the corresponding latitude and longitude were extracted, thereby enabling intelligent extraction of the position, intensity, and width of ocean fronts. Here, intensity refers to the temperature gradient magnitude, and the width was calculated as twice the distance from the centerline to the boundary. Specifically, the centerline is extracted by computing the morphological skeleton of the predicted binary front mask. The width at each point along the skeleton is then calculated as twice the value of the Euclidean distance transform at that point, which represents the shortest distance from the centerline point to the mask boundary. The reported frontal width is the average of these per-point width values over the entire skeleton. As shown in Fig. 8, the intensity and width of ocean fronts identified by traditional and deep learning methods were also examined. The numerical results are shown in Table 5. In terms of the intensity of a single ocean front, the table presents both the gradient-based and deep learning–based measurements,

which are expressed in degrees °C/km with an error of 0.013 °C/km. The width of a single ocean front detected by the gradient and deep learning methods is measured in kilometres with an error of 0.155 km. These results indicate that the deep learning method is consistent with the gradient detection method in terms of capturing ocean fronts characteristics. Overall, these findings highlight the effectiveness of the deep learning approach in ocean front detection.

Table 5. Precision indicators of single ocean front characteristics

Statistical indicators	Traditional methods	Deep learning	Error
single ocean front intensity (℃/km)	0.112	0.125	0.013
single ocean front width (km)	27.124	27.279	0.155

4.4 Analysis of seasonal changes and spatiotemporal characteristics

Research on the seasonal patterns of ocean fronts is extremely important for better understanding the Earth's climate system, as it helps to gain a deeper understanding of ocean circulation and its impact on seawater temperature, salinity, and nutrient distribution, which is crucial for ecosystems, fisheries, and marine resource management.

Ocean front detection results for the entire year of 2023 are divided by season: spring (March, April, and May), summer (June, July, and August), autumn (September, October, and November), and winter (December, January, and February). In addition, the seasonal averages were calculated to obtain the spatial and temporal distributions of ocean fronts during each season. In terms of the seasonal distribution, ocean fronts activity is most frequent and most common in the winter, followed by the autumn. Spring and summer exhibit relatively weaker gradient magnitudes and less extensive frontal structures, with the weakest signals observed in summer. In terms of frontal activity inferred from gradient intensity, the order, from weakest to strongest, is summer < spring < autumn < winter. Regarding spatial distribution, ocean fronts are more active in nearshore waters. In the South China Sea, ocean fronts are concentrated primarily between Hainan and the Taiwan Strait, with a higher frequency of ocean fronts near the Taiwan Strait. In spring and summer, ocean fronts activity in the South China Sea is relatively inactive, with fewer ocean fronts. In terms of seasonal and spatial distribution characteristics, the results align with prior observations (Hickox et al., 2000).

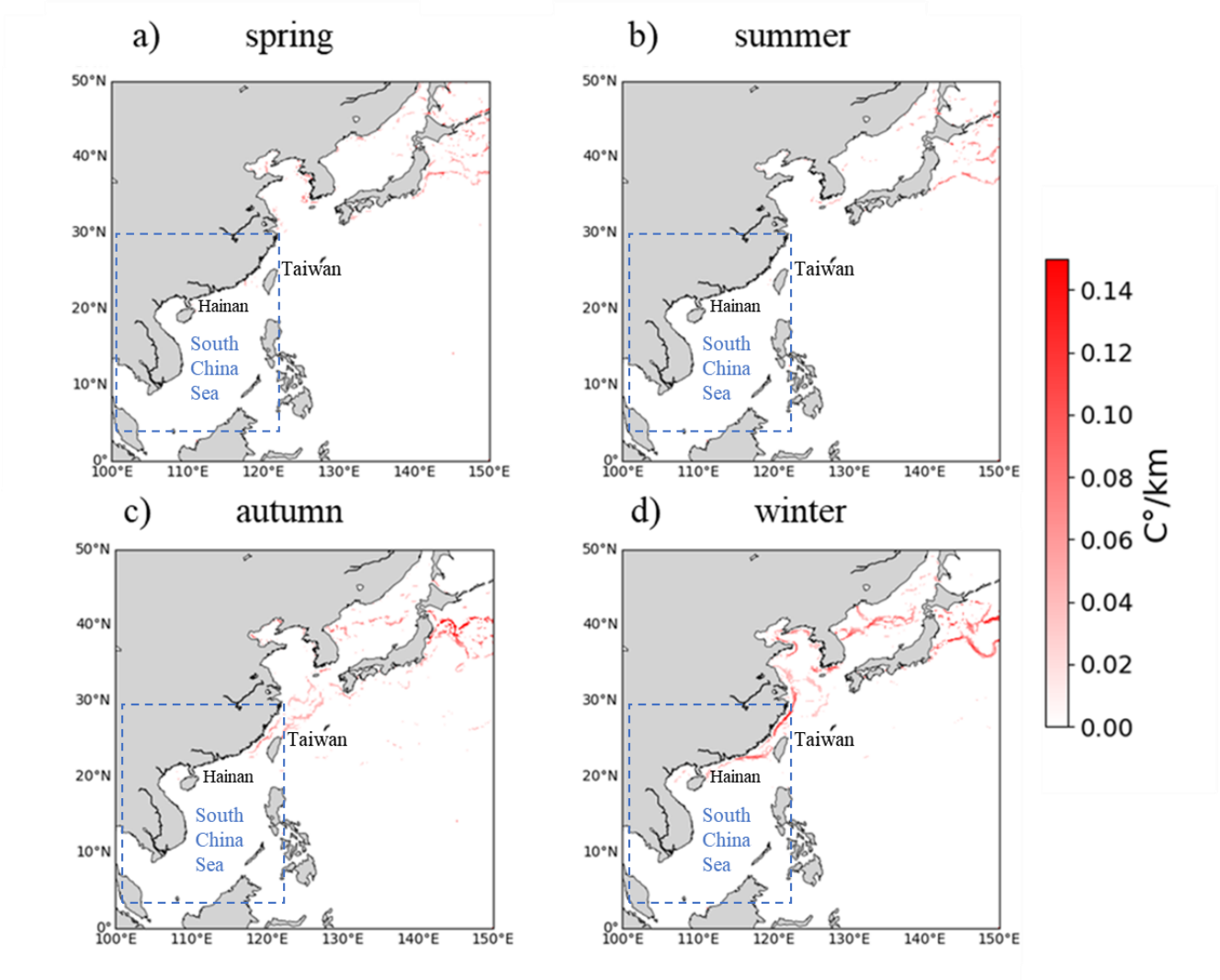

Figure 9. Seasonal spatial-temporal distribution map of ocean fronts in 2023 (The blue dashed box indicates the South China Sea)

4.5 Discussion

4.5.1 Data source limitations

Although the model was trained and evaluated primarily on high-quality L4 reanalysis data (GLORYS12V1) and multi-sensor L3 satellite SST data, its performance may vary when applied to other data sources with different characteristics. In scenarios where the model is deployed on lower-quality data (e.g., single-sensor L2 satellite observations with potential noise, gaps due to cloud cover, or inconsistent spatial coverage), detection accuracy could be affected. Such data may introduce artifacts or missing values that the model has not encountered during training, potentially leading to degraded performance.

Furthermore, meteorological conditions such as wind, clouds, and precipitation may affect the clarity and visibility of satellite images. Adverse weather conditions may cause ocean fronts to be blurry or make their detection in images difficult. Waves, storm surge, eddies, and currents also affect the quality of satellite images. These factors may cause image noise or distortion, making the detection of spikes more difficult. As the performance of deep learning models depends on the available data, more high-quality data and ground truth data can provide better model training and validation.

4.5.2 Model errors

The model errors mainly stem from four aspects: (1) Insufficient model complexity: The selected deep learning model is not sufficiently complicated to capture complex ocean fronts patterns, which can lead to errors. (2) Overfitting or underfitting: overfitting refers to the model performing well on training data but not well on new data, which may occur because the model is too complex and learns the noise in the training data. Underfitting occurs because the model is too simple to capture the complexity of the data. Thus, unreasonable learning rate settings can also affect the accuracy of detection. (3) Inaccurate labels: If the data labels used for training the model are inaccurate or the labeling process is not precise enough, the model will learn the wrong patterns. (4) Lack of sufficient training data: If the amount of ocean fronts data available for training is limited, the model may not be able to fully learn the various features of the front, resulting in errors.

4.5.3 Impact of the marine environment

Oceanographic conditions: Ocean fronts typically occur at boundaries between different water masses, such as cold and warm currents or salinity gradients. Rapid changes in temperature and salinity gradients may affect the spatial structure and position of the fronts, and deep learning models should be able to adapt to these variations.

Seasonal and temporal variations: The position and intensity of ocean fronts may vary significantly across different seasons and time periods. Deep learning models need to be able to capture these seasonal differences.

Subsurface conditions: Ocean fronts typically exist not only at the ocean surface but also extend to the subsurface. Subsurface conditions, such as temperature, salinity, and water flow, can also affect the front properties. If relevant subsurface data are available, incorporating them into model training may help improve the front detection accuracy.

In summary, errors in the detection results when applying deep learning to ocean fronts result from the combined influence of multiple factors, such as the data quality, data label accuracy, data bias, model complexity, overfitting or underfitting, and training data volume. To improve the accuracy of ocean fronts detection, it is necessary to address these factors and continuously optimize the model and data. Future research should focus on addressing these challenges. This process will include developing strategies to obtain more labeled data, improving the model's robustness to environmental factors, and exploring the potential of integrating different data sources to increase the accuracy and applicability of the method.

5 Data availability

The 30-year ocean front dataset (1993–2023) for the Northwest Pacific is available at https://doi.org/10.5281/zenodo.16921277 (Yuan Niu, 2025).

6 Conclusions

As an important ocean phenomenon, the rapid and accurate detection of ocean fronts is highly important for marine ecology, fishery resources, and typhoon path prediction. Given the scarcity of ocean fronts data, this study constructed a manually labeled ocean front dataset of approximately 5,000 samples spanning 30 years and proposed a deep learning-based method for ocean front detection by using the Mask R-CNN model. The experimental results show that this method can achieve automatic ocean front detection with an accuracy exceeding 90%. To improve the model’s detection accuracy, cross-

validation techniques were used to optimize the algorithm's hyperparameters, including the learning rate, batch size, and loss function weights, to achieve better performance. Additionally, data augmentation techniques such as rotation, scaling, flipping, and brightness adjustment were applied to enhance the robustness of the model. The use of 30 years of sea surface temperature data provides strong support for a deeper understanding of the seasonal and interannual variations in ocean fronts. By analysing long-term time series data, trends in ocean fronts changes can be identified, including their seasonal migration and potential climate-driving factors. Overall, the results of this study demonstrate the effectiveness of the proposed method in terms of detecting and extracting ocean fronts and highlight the need for further research and development to fully realize its potential for broad applications in oceanography and climatology.

Author contributions. XZ and DZ conceived this study. YN and DZ collected the datasets. YN implemented the research and wrote the original draft of the paper. All the authors discussed the results and revised the manuscript.

Competing interests. The contact author has declared that none of the authors has any competing interests.

Acknowledgements. The authors would like to thank the editors and anonymous reviewers for their valuable comments. The authors thank the Copernicus Marine Environment Monitoring Service (CMEMS) for providing the GLORYS12V1 ocean reanalysis dataset, which is based on the NEMO model and driven by ECMWF ERA-Interim and ERA5 reanalyses.

Financial support. This work was supported in part by the Key Research and Development Program, sponsored by the Ministry of Science and Technology (MOST), under Grant 2023YFC3107701 and Grant 2023YFC3107901; in part by the National Natural Science Foundation of China under Grant 42375143.

References

Azevedo, M. H., Rudorff, N., and Aravéquia, J. A.: Evaluation of the ABI/GOES-16 SST Product in the Tropical and Southwestern Atlantic Ocean, Remote Sens., 13, 192, https://doi.org/10.3390/rs13020192, 2021.

Belkin, I. M. and O'Reilly, J. E.: An algorithm for oceanic front detection in chlorophyll and SST satellite imagery, J Marine Syst, 78, 319-326, https://doi.org/10.1016/j.jmarsys.2008.11.018, 2009.

Belkin, I. M., Cornillon, P. C., and Sherman, K.: Fronts in Large Marine Ecosystems, Prog. Oceanogr., 81, 223-236, https://doi.org/10.1016/j.pocean.2009.04.015, 2009.

Cayula, J.-F. and Cornillon, P.: Edge detection algorithm for SST images, J. Atmos. Oceanic Technol., 9, 67-80, https://doi.org/10.1175/1520-0426(1992)009<0067:EDAFSI>2.0.CO;2, 1992.

Chen, C.: Chemical and physical fronts in the Bohai, Yellow and East China seas, J Marine Syst, 78, 394-410, https://doi.org/10.1016/j.jmarsys.2008.11.016, 2009.

Chen, Y., Tang, L., Kan, Z., Bilal, M., and Li, Q.: A novel water body extraction neural network (WBE-NN) for optical high-resolution multispectral imagery, J. Hydrol., 588, https://doi.org/10.1016/j.jhydrol.2020.125092, 2020.

Chronis, T.: Evaluating the Detection of Mesoscale Outflow Boundaries Using Scatterometer Winds at Different Spatial Resolutions, Remote Sens., 13, https://doi.org/10.3390/rs13071334, 2021.

Davis, L. S.: A survey of edge detection techniques, Comput. Graph. Image Process., 4, 248-270, https://doi.org/10.1016/0146-664X(75)90012-X, 1975.

Dice, L. R.: Measures of the amount of ecologic association between species, Ecology, 26, 297-302, https://doi.org/10.2307/1932409, 1945.

Diehl, S. F., Budd, J. W., Ullman, D., and Cayula, J.-F.: Geographic window sizes applied to remote sensing sea surface temperature front detection, J. Atmos. Oceanic Technol., 19, 1105-1113, https://doi.org/10.1175/1520-0426(2002)019<1105:GWSATR>2.0.CO;2, 2002.

Felt, V., Kacker, S., Kusters, J., Pendergrast, J., and Cahoy, K.: Fast Ocean Front Detection Using Deep Learning Edge Detection Models, IEEE Trans. Geosci. Remote Sens., https://doi.org/10.1109/TGRS.2023.3276374, 2023.

Gruber, N., Lachkar, Z., Frenzel, H., and Marchesiello, P.: Mesoscale eddy-induced reduction in eastern boundary upwelling systems, Nat. Geosci., 4, 787-792, https://doi.org/10.1038/NGEO1273, 2011.

He, K., Gkioxari, G., Dollar, P., and Girshick, R.: Mask R-CNN, IEEE Trans. Pattern Anal. Mach. Intell., 386-397, https://doi.org/10.1109/TPAMI.2018.2844175,

Hickox, R., Belkin, I., Cornillon, P., and Shan, Z.: Climatology and seasonal variability of ocean fronts in the East China, Yellow and Bohai Seas from satellite SST data, Geophys. Res. Lett., 27, 2945-2948, https://doi.org/10.1029/1999GL011223, 2000.

Li, Q., Fan, Z., and Zhong, G.: BEDNet: Bi-directional Edge Detection Network for Ocean Front Detection, Lect. Notes Comput. Sci., https://doi.org/10.1007/978-3-030-63820-7_35,

Li, Y., Liang, J., Da, H., Chang, L., and Li, H.: A Deep Learning Method for Ocean Front Extraction in Remote Sensing Imagery, IEEE Geosci. Remote Sens. Lett., 19, https://doi.org/10.1109/LGRS.2021.3081179, 2022.

Lin, T.-Y., Maire, M., Belongie, S., Hays, J., Perona, P., Ramanan, D., Dollár, P., and Zitnick, C. L.: Microsoft coco: Common objects in context, Eur. Conf. Comput. Vis., 740-755, https://doi.org/10.1007/978-3-319-10602-1_48,

Nieto, K., Demarcq, H., and McClatchie, S.: Mesoscale frontal structures in the Canary Upwelling System: New front and filament detection algorithms applied to spatial and temporal patterns, Remote Sens. Environ., 123, 339-346, https://doi.org/10.1016/j.rse.2012.03.028, 2012.

Niu, R., Tan, Y., Ye, F., Gong, F., Huang, H., Zhu, Q., and Hao, Z.: SQNet: Simple and Fast Model for Ocean Front Identification, Remote Sens., 15, 2339, https://doi.org/10.3390/rs15092339, 2023.

Nogueira, K., Penatti, O. A. B., and Santos, J. A. D.: Towards Better Exploiting Convolutional Neural Networks for Remote Sensing Scene Classification, Pattern Recognit., 61, 539-556, https://doi.org/10.1016/j.patcog.2016.07.001, 2016.

Oram, J. J., McWilliams, J. C., and Stolzenbach, K. D.: Gradient-based edge detection and feature classification of sea-surface images of the Southern California Bight, Remote Sens. Environ., 112, 2397-2415, https://doi.org/10.1016/j.rse.2007.11.010, 2008.

Ping, B., Su, F., Meng, Y., Fang, S., and Du, Y.: A model of sea surface temperature front detection based on a threshold interval, Acta Oceanol. Sin., https://doi.org/10.1007/s13131-014-0502-x, 2014.

Reichstein, M., Camps-Valls, G., Stevens, B., Jung, M., and Denzler, J.: Deep learning and process understanding for data-driven Earth system science, Nature, 556, 195-204, https://doi.org/10.1038/s41586-019-0912-1, 2019.

Roa-Pascuali, L., Demarcq, H., and Nieblas, A.: Detection of mesoscale thermal fronts from 4 km data using smoothing techniques: Gradient-based fronts classification and basin scale application, Remote Sens. Environ., 164, 225-237, https://doi.org/10.1016/j.rse.2015.03.030, 2015.

Ruiz, S., Claret, M., Pascual, A., Olita, A., Troupin, C., Capet, A., Tovar-Sanchez, A., Allen, J., Poulain, P.-M., Tintore, J., and Mahadevan, A.: Effects of Oceanic Mesoscale and Submesoscale Frontal Processes on the Vertical Transport of Phytoplankton, J. Geophys. Res. Oceans, 124, 5999-6014, https://doi.org/10.1029/2019JC015034, 2019.

Saldías, G. S., Hernandez, W. J., Lara, C., Muoz, R., and Soto-Mardones, L.: Seasonal Variability of SST Fronts in the Inner Sea of Chiloé and Its Adjacent Coastal Ocean, Northern Patagonia, Remote Sens., 13, https://doi.org/10.3390/rs13020181, 2021.

Shaw, A. and Vennell, R.: Measurements of an Oceanic Front Using a Front-Following Algorithm for AVHRR SST Imagery, Remote Sens. Environ., 75, 47-62, https://doi.org/10.1016/S0034-4257(00)00155-3, 2001.

Wada, K.: wkentaro/labelme: v4.6.0 (v4.6.0), Zenodo [code], https://doi.org/10.5281/zenodo.5711226, 2021.

Wang, F. and Liu, C.: An N-shape thermal front in the western South Yellow Sea in winter, Chin. J. Oceanol. Limnol., 27, 896-906, https://doi.org/10.1007/s00343-009-9045-y, 2009.

Wang, X. L. and Wang, C. L.: Extraction of Ocean Fronts Based on Empirical Mode Decomposition, Appl. Mech. Mater., 701-702, 303-307, https://doi.org/10.4028/www.scientific.net/AMM.701-702.303, 2015.

Yang, C., Rongshuang, F., Muhammad, B., Xiucheng, Y., Jingxue, W., and Wei, L.: Multilevel Cloud Detection for High-Resolution Remote Sensing Imagery Using Multiple Convolutional Neural Networks, Int. J. Geo-Inf., 7, https://doi.org/10.3390/ijgi7050181, 2018.